Eur. Phys. J. Special Topics **208**, 305–318 (2012)

DOI: 10.1140/epjst/e2012-01626-y

THE EUROPEAN PHYSICAL JOURNAL SPECIAL TOPICS

Review

Characterization of organic thin films with resonant soft X-ray scattering and reflectivity near the carbon and fluorine absorption edges

H. Ade[a]

Dept. of Physics, NCSU, Raleigh, NC 27596, USA

Received 15 February 2012 / Received in final form 23 March 2012
Published online 15 June 2012

Abstract. The use of soft X-rays near the carbon absorption edge (∼270–300 eV) for small angle X-ray scattering and X-ray reflectivity experiments has significantly expanded the scientific capabilities to investigate thin films of soft matter that are primarily composed of carbon and low Z heteroatoms. In this perspective, we will delineate the basic operating principles and underlying physics of these methods and exemplify their impact by discussing a few recent applications. An extension of these methods to the fluorine edge is also included, demonstrating that the general concepts are also applicable to absorption edges of hetero atoms in soft matter. A short perspective of some future developments is provided.

1 Introduction and background

High performance materials often combine the complementary properties of multiple components and are naturally or intentionally nano-structured to capture the synergy that the combination of materials can provide. Examples are organic solar cells in which a donor and acceptor material are combined in an intricate nano-morphology to achieve high efficiency [1], and block copolymers with controlled nanostructure used for templating or unique mechanical properties [2]. Use of highly engineered materials can be ubiquitous, such as the use of triblock copolymers as shock-absorbers and adhesives in many shoes. The desired nanostructures can be achieved by top-down methods (e.g. lithography), but in soft matter systems structuring is typically achieved through bottom-up approaches that utilize self-assembly processes and mechanisms. To fully understand and control structure-performance relationships and their dependence on processing, morphological or structural characterization at the sub-100 nm or even the ∼1 nm length scale is required. Scattering methods are frequently employed to provide the needed information, with the range of their utility limited by the contrast between constituent materials, length scales probed through the accessible q-range, possible radiation damage, and control of the sample environment [3,4]. During the last decade or so, soft X-ray scattering has been shown to exhibit a combination

[a] e-mail: harald_ade@ncsu.edu

of attributes that makes it well suited to investigate a range of materials. Resonant scattering was initially known to have great utility for the characterization of magnetic materials [5]. Its unique characterization advantages were employed for the first time on organic materials in the work of Wang et al [6] and Mitchell et al. [7], which showed that tunable and high sensitivity to constituent materials and specific interfaces can be achieved in reflectivity as well as in transmission experiments from very thin films. The characterization of structured nanoparticles [8] and block copolymers [9] followed, The utility was subsequently extended to suspensions and the range of contrast between various materials, including hard carbon materials, was further expanded and utilized [10–17]. We will review the strengths of resonant soft X-ray scattering from organic materials and exemplify its utility by highlighting a number of recent applications. The methods described should be applicable to all materials with elements that have strong absorption edges in the 90–900 eV energy range.

2 Contrast mechanism with soft X-rays

Conventional small angle X-ray scattering (SAXS) generally relies on electron density differences for scattering contrast [3,4]. Near an absorption edge, anomalous scattering (ASAXS) enhancements can be exploited that provide both improved sensitivity to specific elements and improved scattering intensity [18,19]. In the soft X-ray energy range, these enhancements are not referred to as "anomalous", but as resonant scattering. For soft matter application, resonant scattering is often referred to as R-SoXS (Resonant Soft X-ray Scattering) and resonant reflectivity as R-SoXR, keeping in line with prior nomenclature from the soft X-ray magnetic and spectroscopic community [5,20,21] and providing a pronounceable acronym (arh-sox). The physical basis of the contrast mechanism is the same than for ASAX. The translation into a solid state picture and the general advantages of R-SoXS have been described previously [10,12]. Basically, the interaction of X-rays with a material is encoded in the complex index of refraction $n(E) = 1 - \delta(E) + i\beta(E)$, where E is the photon energy, δ is the index decrement, and β is the extinction coefficient. We refer to δ and β as optical constants. $n(E)$ is the most immediate quantity to consider, as it takes into account the composition and density of the actual samples. In the forward scattering or long wavelength limit, the two energy dependent terms of $n(E)$ are related to the complex scattering factor $f = f_1 + if_2$ ($= f_o + \Delta f' + i\Delta f''$ in anomalous SAXS terminology) through $(\delta + i\beta) = \alpha\lambda^2(f_1 + if_2)$, where λ is the photon wavelength and $\alpha = n_a r_e/2\pi$, with n_a being the number density of atoms, and r_e is the classical radius of the electron. δ and β (or f_1 and f_2) are related to each other by a Kramers-Kronig transform. Consequently, the strong dependence of NEXAFS on specific functional groups generally observed for organic materials translates into equally strong and functional group-specific energy dependence of δ. This is illustrated in Fig. 1, which shows the optical constants δ and β for polyfluorene copolymers poly(9,9-dioctylfluorene-co-bis(N,N′-(4,butylphenyl))bis(N,N′-phenyl-1,4-phenylene)diamine) (PFB) and poly(9,9-dioctylfluorene-co-benzothiadiazole) (F8BT). Despite similar chemical functional groups with a highly aromatic backbone and aliphatic side-chains, significant spectral differences are observed, particularly near 285 eV, that reflect the specific unsaturation of the bonding in the backbone and the delocalization of the electronic structure.

The quantity $(\Delta\delta^2 + \Delta\beta^2)$ determines the scattering contrast between material phases (composition or orientation). The scattering intensity $I(q)$ is proportional to $E^4(\Delta\delta^2 + \Delta\beta^2)$. This dependence has two major consequences: i) "bond-specific" or functional group specific scattering can be achieved in R-SoXS by judicious choice of photon energy [6–8], in a manner analogous to NEXAFS microscopy of polymers

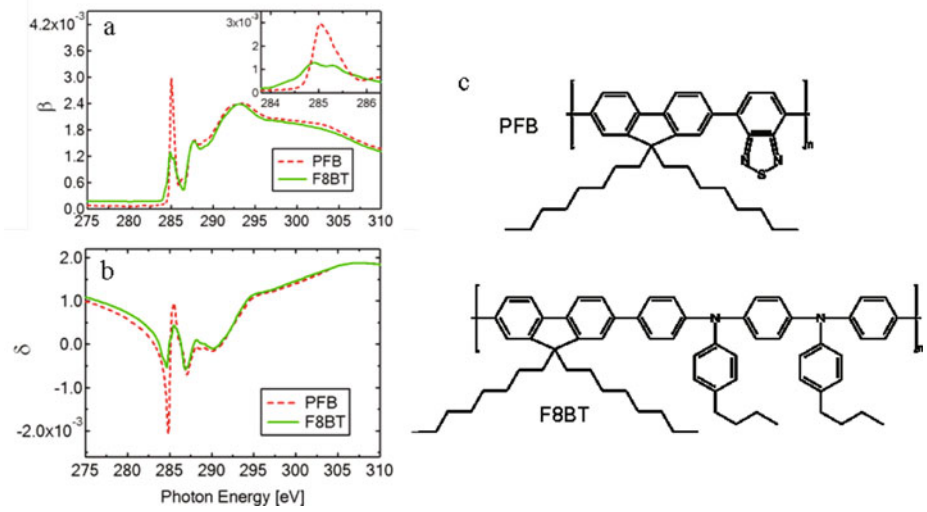

Fig. 1. Optical constants β (a) and δ (a) near the carbon 1s absorption edge for polymers PFB and F8BT as indicated, along with chemical structure of these polymers (c).

[22,23], ii) in addition, $\Delta\delta^2 + \Delta\beta^2$ overcomes or at least neutralizes the E^4 factor that would favor use of higher energy photons and orders of magnitude larger scattering intensity can be achieved near the carbon edge relative to photons with $E \sim 10\,\text{keV}$ as used in conventional SAXS [7,11]. This affords the opportunity to get useable scattering intensities in transmission even from rather thin films only 20–200 nm in thickness [7–9,24]. More recently, it has been pointed out and demonstrated that R-SoXS furthermore has unique contrast to bond orientation if polarized light and polarization control of the incident photons are available [24].

To first order, material pairs exhibiting strong differences in their NEXAFS spectra yield high scattering contrast. Since NEXAFS spectra can be utilized to predict contrast, they are a key ingredient to design R-SoXS experiments and guide data analysis. Compilations of NEXAFS spectra from polymers by Dhez et al. [25], Kikuma and Tonner [26], and Watts et al. [27], and a delineation of the evolutionary trends of the spectral signature of carbonyl functional groups as the nearest neighbor environment is changed progressively and systematically from a ketone to a carbonate group [28] are thus very useful. Complementary compilations of NEXAFS from molecules used in solar cells [29] and exploration of subtle difference between urea and urethane group [30] and even isomers of phthalates [31] are also available.

The reader is referred to the literature for more details on contrast and optical constants [10,12].

3 Insights from resonant soft X-ray scattering

After the initial demonstrations of R-SoXS and R-SoXR and application involving nanoparticles and bilayer model systems [6,8], most of the recent applications of these methods have focused on characterizing organic devices [13,32–39]. The primary reasons for using R-SoXS in these applications is that NEXAFS microscopy and other methods do not have the spatial resolution or chemical sensitivity required to asses the fine details present at the nanometer scale. Analysis of R-SoXS data is analogous to that of SAXS and SANS and sophisticated analysis methods common to all scattering methods can be used to determine, for example, pair distribution and other

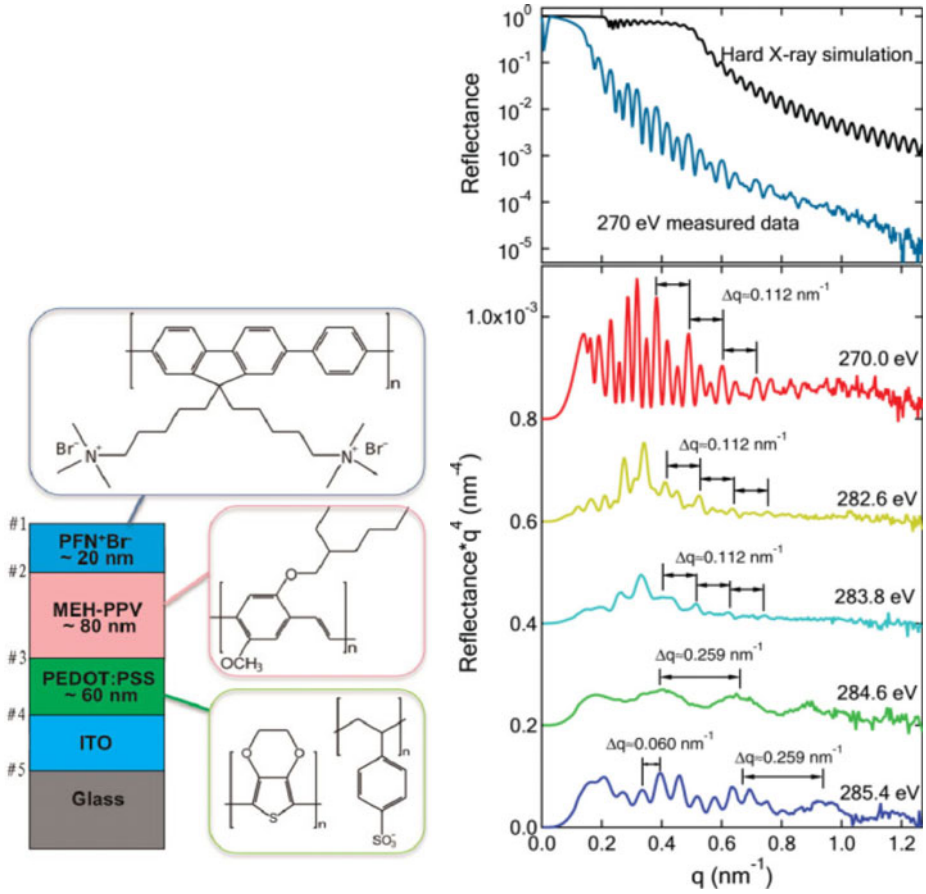

Fig. 2. (Left) schematic of FNBr/MEH-PPV/PEDOT:PSS/ITO/glass multilayer and molecular structures of the materials used. (Right) reflectance of this multilayer at selected photon energies as indicated. (Top) simulation at 8000 eV of such a multilayer with perfect interfaces. Note the scaling by q^4. Figure reproduced from ref. [46].

correlation functions and to measure or estimate the purity of domains [3,4,40]. The sensitivity to the smallest length scale is particularly pronounced in θ-2θ reflectometry experiments, where 0.1 nm accuracy in determining interfacial widths can be achieved even with the use of X-rays that have wavelengths much larger than that [6,10,13,36].

3.1 Characterization of bilayer and multilayers used in organic devices

In polymer LEDs (PLEDs), two different polymers are often used to provide flexibility in optimizing the injection and transport of electrons and holes. Laterally phase separated blends can be used, but polymer multilayers are frequently employed [41–45]. The fabrication of multilayered PLEDs is tremendously simplified with the use of charged conjugated polyelectrolytes (CPE) such as PFNBr (See Fig. 2 for chemical structure). These are polar electron transport materials that can be cast directly from a polar solvent onto non-polar hole transport materials such as poly[2-methoxy-5-(2'-ethylhexyloxy)-p-phenylene vinylene] (MEH-PPV).

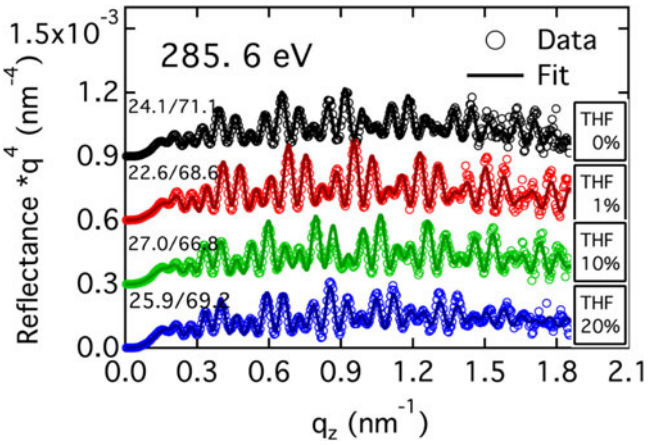

Fig. 3. R-SoXR model refinement (fit) and data acquired at 285.6 eV for PFNBr/MEH-PPV/Si bilayers which had the PFNBr cast from methanol:THF mixtures as indicated. The numbers at the right of the reflectance traces are the layer thicknesses in nm as derived from the fits. Note the scaling by q^4. Data offset for clarity. Figure reproduced from ref. [47].

Figure 2 shows the R-SoXR data for a PFNBr/MEH-PPV/PEDOT:PSS/ITO/glass multilayer device at five photon energies. The general structure of the multilayer and the chemical structures of the materials are also provided in Fig. 2. This multilayer structure is a complete device but for the top electrode. Complicated reflectance patterns arise as a function of photon energy since the reflections from each interface interfere and their respective reflectivity is photon energy dependent. In addition, absorption can play an important and dominant role in R-SoXR. We refer the reader for details to the literature, but include this data here for tutorial purposes to illustrate just how much variation in the reflectance can be achieved and observed by changes in the photon energy. The simulations at 8000 eV do not show any modulations in the Kiessig fringes, thus clearly demonstrating the lack of contrast for all polymer/polymer interfaces when hard X-rays are used. A more complete analysis of this multilayer was recently accomplished [47].

That casting using differential solvents does not disrupt the initial layer in negative ways or is even beneficial was an assumption underlying the development of many CPE materials. Transmission electron microscopy (TEM) studies [48] have indeed shown that only materials having opposite polarity and cast from solvents of matching polarity yield relatively sharp interfaces and well developed bilayer structures. Quantitative measurements of the interfacial width for very sharp interfaces are, however, difficult with TEM and the interface was estimated to be ~2 nm wide. Conventional X-ray reflectivity has little sensitivity to investigate this material pair as shown in Fig. 2 [46]. In contrast, R-SoXR has excellent contrast and was used to show with high precision that the differential casting of CPEs on top of MEH-PPV yields sharp and smooth interfaces with an RMS width of only 0.8 nm [13].

Furthermore, R-SoXR was used to show that the interfacial width can be controlled by either variations is the solvent mixtures used or a number of annealing protocols [47]. R-SoXR results, i.e. data at 285.6 eV and model refinements, of PFNBr/MEH-PPV/Si bilayers cast from different solvent mixtures are displayed in Fig. 3. The reflectance profiles exhibit clear Kiessig fringe modulations that indicate a bilayer structure. The interfacial width changed appreciably as a function of solvent polarity only for the highest tetrahydrofurane (THF) content. This can be qualitatively appreciated by the reduction in fringe amplitude at high q for the 20%:80% THF:methanol mixture. Model refinement showed that the width increases to 1.2 nm

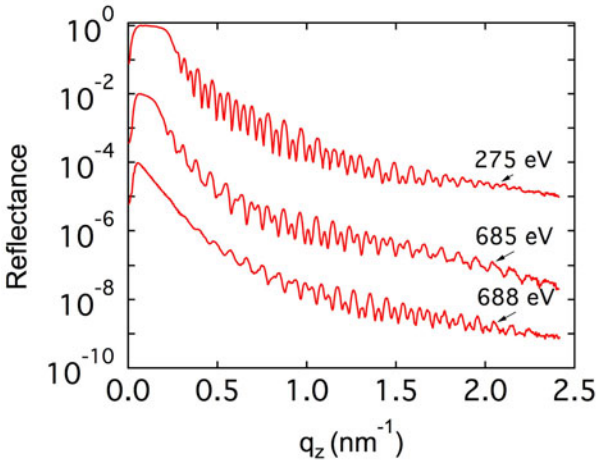

Fig. 4. R-SoXR data of bilayer CYTOP on P(NEI2OD-T2) on a very thin oxide layer covered silicon substrate acquired at photon energies of 275 eV, 685 eV and 688 eV. Figure courtesy of Hongping Yan (NCSU).

from the 0.8 nm observed for 100% methanol. The 1% and 10% THF solutions yield essentially the same sample as if pure methanol solvent was used. These results are not unexpected. PFNBr has been specifically designed to allow differential casting from methanol, a poor solvent for MEH-PPV. The MEH-PPV layer surface is indeed not disturbed much with the use of methanol. Since THF can dissolve both PFNBr (top layer) and MEH-PPV (bottom layer), sufficient THF (i.e. 20%) during casting of the PFNBr does, however, broaden the interface.

R-SoXR has also been successfully used to study planar photovoltaic heterojunctions based on the polyfluorene copolymers PFB and F8BT. By obtaining quantitative information of morphology, photoluminescence quenching and device performance, it was possible to examine the competing effects of exciton dissociation and charge separation and recombination, and to show that sharp, non-equilibrium interfaces produce the best device performance [36]. Similarly, organic thin film transistors (TFTs) bilayers have been successfully characterized. Devices consisting of a dielectric top layer of either polystyrene (PS), poly(methyl meth acrylate) (PMMA) or CYTOP CTL-809M (a fluorinated polymer from Asahi Glass) and a bottom layer of poly{[N,N9-bis(2-octyldodecyl)-naphthalene-1,4,5,8-bis(dicarboximide)-2,6-diyl]-alt-5,59-(2,29-bithiophene)} (P(NDI2OD-T2), Polyera Corporation Active Ink N2200) were characterized and qualitatively compared [39,47]. P(NDI2OD-T2) is a newly developed high-mobility electron transporting polymer [49,50]. A correlation between turn-on voltage and interfacial width and an anticorrelation between activation energy and width for the different dielectrics was observed [39]. Furthermore, the effect of differential casting in these TFTs on the initial interfacial width was investigated. The R-SoXR investigations on CYTOP/P(NDI2OD-T2) also clearly demonstrated that R-SoXR methods can be successfully extended to the fluorine 1s absorption edge [39,47]. Fig. 4 shows R-SoXR data of a 75 nm/55 nm CYTOP/P(NDI2OD-T2) bilayer at 275 eV, 685 eV and 688 eV. At 275 eV, Kiessig fringes corresponding to the surface and substrate interfaces dominate. In contrast, at 685 eV and 688 eV, modulations clearly show more pronounced modulations and thus higher sensitivity to the buried CYTOP/P(NDI2OD-T2) interface.

3.2 Characterization of bond orientation

It is well known that NEXAFS spectra exhibit a strong angular dependence if there is a preferential orientation or anisotropy in the material [51]. This linear dichroism can also be exploited in scattering/reflectivity and the combination of dichroism and reflectivity has been used for the first time to study depth profiles of molecular orientation in soft matter thin films with nanometer resolution. poly(2-{4-[(4-cyanophenoxy)carbonyl]phenoxy}ethyl acrylate), a polymer with liquid-crystalline side chains, has been used in this study [24]. Strong differences in the reflectivity between s and p polarization geometries were recorded in the vicinity of the absorption resonance associated with the phenylene and nitrile π systems present in the polymer. Fringes in $R(q)$ for s and p polarization were observed to be shifted with respect to each other. To highlight these differences, the asymmetry, defined as $(R_p - PR_s)/(R_p + PR_s)$, was considered, where $P = \cos^2 2\theta$ denotes the Lorentz polarization factor. This asymmetry parameter shows clear energy and polarization dependence (see Fig. 5). One can readily see that the degree and direction of these shifts, as well as the differences in the oscillation amplitudes, depend strongly on the energy and polarization of the incident X- rays. With increasing scattering angle, the differences tend to decrease and finally vanish at normal incidence where the projections of the electric-field vectors on the surface plane become equal.

Polarization dependent scattering has also been exploited in a transmission geometry to probe in-plane bond anisotropy in TFTs and organic photovoltaic (OPV) systems [52]. This strong polarization dependent contrast mechanism is absolutely unique to soft X-rays. Neither small angle neutron scattering, nor conventional SAXS have such sensitivity to orientational bond anisotropies, which makes R-SoXS unique amongst those scattering methods that can probe small length scales.

3.3 In-plane morphologies in organic solar cells

Recent rapid improvements in organic solar cell efficiency might make these devices a source of abundant electricity if some additional improvements in efficiency and device lifetime can be made. The 3-dimentional nanoscale morphology in the active layer required for efficient devices is referred to as a bulk heterojunction (BHJ). Typically, it is assumed that lateral structures on the ∼10 nm length scale are required in order to match the diffusion length of the exciton that is created with the absorption of a photon. At the same time, thicknesses in excess of 100 nm are required for efficient photon absorption. Furthermore, cheap, non-equilibrium processing methods such as spin-casting and printing are employed. Due to this complexity, determining the detailed structure-property relationships of such devices has been a major challenge. R-SoXS is one of the advanced tools that can provide insights [32,33,37,38]. It has been used to characterize the in-plane structure of a number of thin films used in organic solar cells. This includes blends of poly(3-hexylthiophene) (P3HT) and [6,6]-phenyl-C 61 butyric acid methyl ester (PCBM) [32] and interdiffused bilayers of P3HT and PCBM [33], as well as all-polymer devices based on PFB and F8BT [32], and P3HT and P(NDI2OD-T2) [38]. Despite of a lot empirical progress, fundamental understanding is still lacking. Even for the much studied P3HT:PCBM system, a definitive picture of the morphology is still lacking [33]. Newer, higher performing materials systems require their own comprehensive characterization since the morphological features are proving to be quite different from those found in P3HT:PCBM. For example, the highest performing polymer/fullerene combination involves a copolymer, thieno[3,4-b]thiophene-*alt*-benzodithiophene (PTB7), which when mixed with $PC_{71}BM$ yields efficiencies of ∼8.4% [54]. In order to achieve high performance, solvent additives preferential to PCBM are used. The effect of such additives is shown

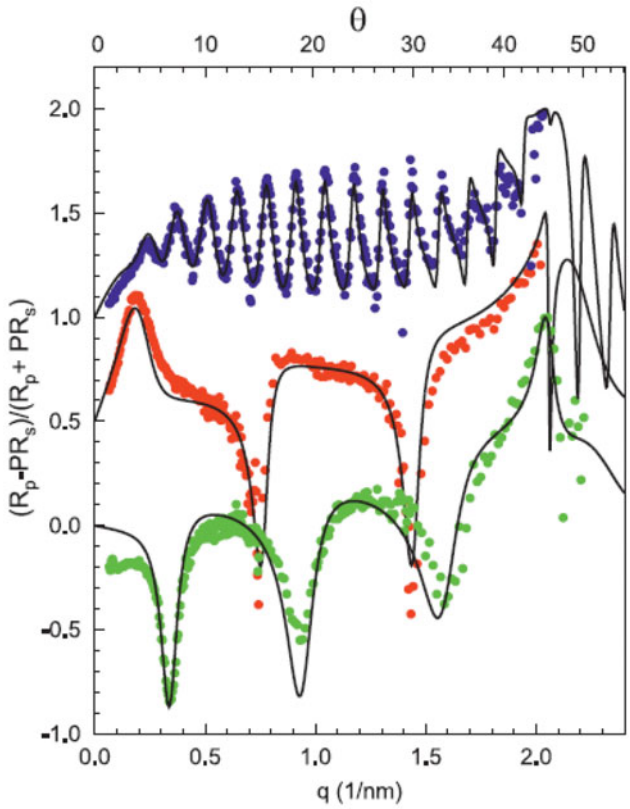

Fig. 5. Asymmetry $(R_p - PR_s)/(R_p + PR_s)$ of the reflectivity data (symbols) and the calculated curves (lines) for a 9.6 nm thick sample of poly(2-{4-[(4-cyanophenoxy)carbonyl] phenoxy}ethyl acrylate) at 285.4 eV (bottom), 284.8 eV (middle), and 49 nm thick sample at 284.8 eV (top). Each curve is vertically offset by 0.5 for clarity. Reproduced from ref. [24].

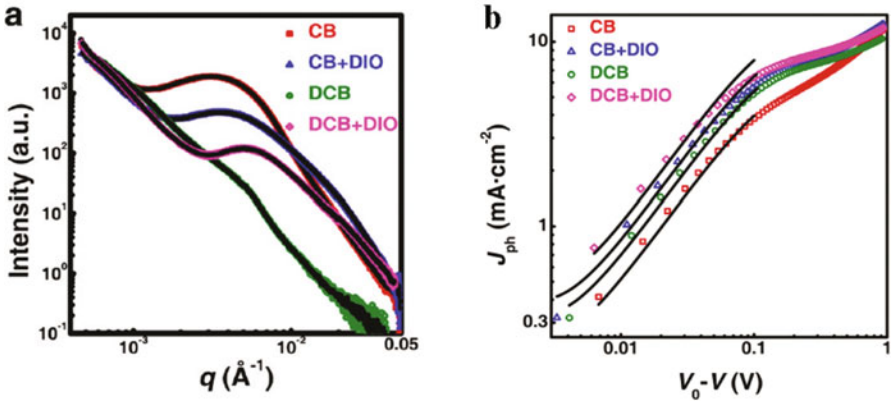

Fig. 6. a) Transmission R-SoXS of ∼80 nm thick PTB7:PCBM films cast from different solvent mixtures, and b) photocurrent device measurements. (Legend: Chlorobenzene (CB), 1,8-diiodooctane (DIO), 1,2-dichlorobenzene (DCB)). Reproduced from ref. [35].

in Fig. 6, where R-SoXS profiles for PTB7/$PC_{61}BM$ films cast using different solvents mixtures reveal clear morphological differences as reflected in the differences in the scattering profiles [35]. R-SoXS utilized X-rays tuned to molecular resonances to enhance material contrast over other scattering sources such as surface roughness. Length scales from several nm to several microns are probed and the morphology and phase separation that yields the greatest number of dissociated excitons at open-circuit can be identified from comparison to device data (Fig. 6(b)). Here, a hierarchy of morphologies, rather than a uniformly structured BHJ was found to work best. Since $PC_{61}BM$ instead of $PC_{71}BM$ was used, the experiments will have to be performed also for $C_{71}BM$ based devices to assess if a hierarchical morphology is truly required to yield devices with PCE ∼8%.

3.4 In-plane block copolymer morphologies

Applications of R-SoXS to systems other than organic devices include the characterization of block copolymers (BCPs) [9,55,56]. We will exemplify the benefit of using energy dependent selective contrast as provided by R-SoXS by reviewing a recent study of a block copolymer with a complex and unique morphology [56]. In BCP, each blocks is composed of the same monomer A and compositionally different blocks, i.e. A and B, are covalently joined to form a single macromolecule. BCPs can self assemble into ordered structures such as lamellae, hexagonally packed cylinders, and body-centered cubic packed spheres. These structures form the basis for templates and scaffolds or provide unique mechanical properties. The most studied materials are AB diblock copolymers. Studies of ABC-type triblock copolymers are far more limited due to their demanding synthesis and complexity, yet, understanding their morphologies and the parameters that control their ordering are essential to fully realize the potential of these materials.

R-SoXS was a critical tool in revealing a novel morphology of the triblock copolymer poly(1,4-isoprene)-block-polystyrene-block-poly(2-vinyl pyridine) (IS2VP) and the differences between bulk and thin films. Panels a and b of Fig. 7 display δ and β of poly(1,4-isoprene) (PI – blue solid line), polystyrene (PS – red dashed line), and poly(2-vinyl pyridine) (P2VP – green dotted line), the constituent blocks of IS2VP. Since the X-ray scattering is proportional to $\Delta\delta^2 + \Delta\beta^2$, the relative scattering contributions of the different blocks can be isolated by judicious choice of photon energy. Consequently, the R-SoXS data of an IS2VP bulk sample exhibits rather different profiles at 250, 280, and 284 eV (Fig. 7(c)). At 280 eV, three scattering peaks are observed that can be assigned to a hexagonally packed structure. At 250 and 284 eV, a single strong scattering peak is observed at $0.16\,\mathrm{nm}^{-1}$ and $0.27\,\mathrm{nm}\,\mathrm{nm}^{-1}$, respectively, indicating that two completely different lattices were observed at these two energies. At 250 eV, X-ray scattering contrast between PS and PI is virtually zero; "index-matching" between these two constituent components is achieved. Consequently, only the lattice of the P2VP in the "PI-PS" matrix is detected (Fig. 7(d)). Conversely, at 284 eV, the contrast between P2VP and PI domains is minimized (Fig. 7(f)). At 280 eV, the index of refraction of all three polymers is different enough to yield significant contract between any two components (Fig. 7(d)). By modulating the scattering profiles in this way and considering form factor effects, R-SoXS revealed two nested, hexagonal arrays of P2VP and PI cylindrical microdomains residing in the PS matrix: The cylindrical microdomains of one component are located at the interstitial sites of the hexagonal array with the larger d spacing that is formed by the other component [56].

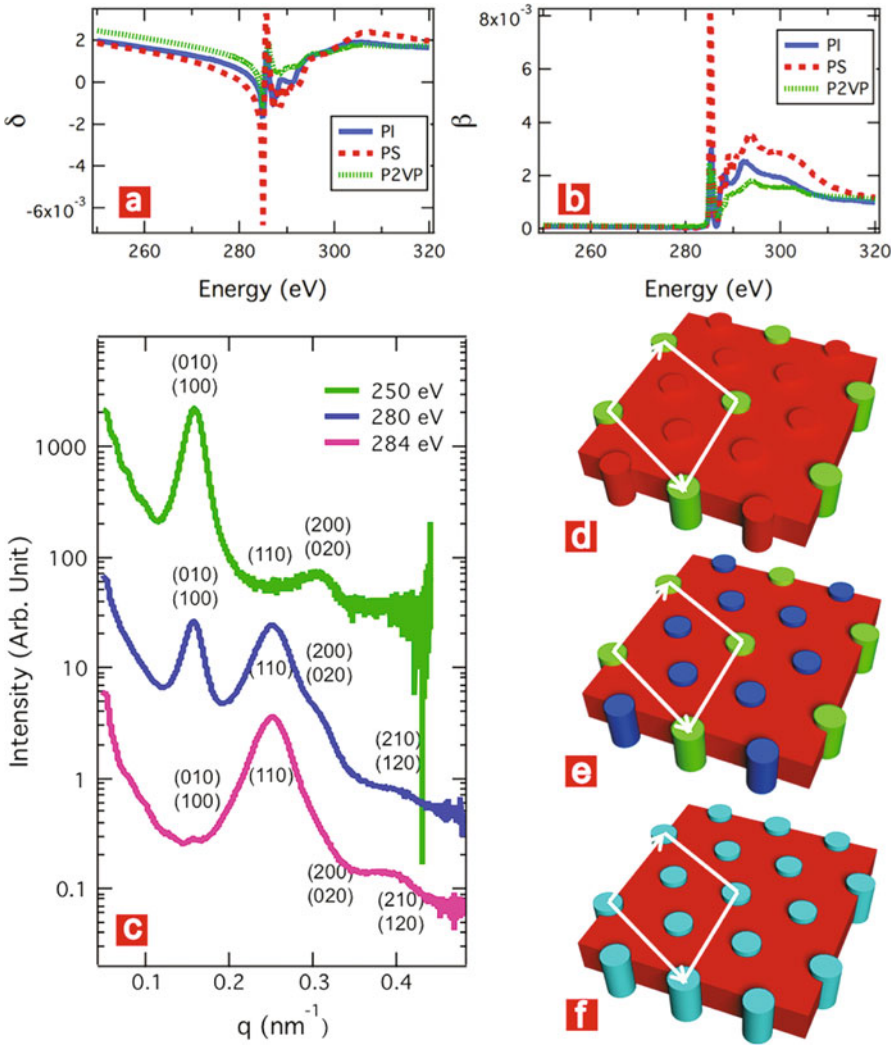

Fig. 7. (a), (b) Index decrement (δ) and extinction coefficient (β) of poly(1,4-isoprene) (blue solid line), polystyrene (red dashed line), and poly(2-vinyl pyridine) (green dotted line), respectively. (c) Scattering intensity at 250, 280, and 284 eV as indicated. (d)–(f) Schematic illustration of hexagonally packed cylindrical morphology of IS2VP triblock copolymer as sensed by 250, 280, and 284 eV photon, respectively. Reproduced from ref. [56].

4 Perspective and outlook

The examples above illustrate some of the unique advantages of R-SoXS/R-SoXR, which include: 1) high and tunable scattering contrast, which leads to 2) high scattering intensity, which in turn 3) allows single 20–200 nm thin films to be studied in transmission; 4) the long wavelength used makes it easy to acquire high quality low q data, and 5) polarization dependence provides unique contrast to investigate bond orientation anisotropy. These are powerful attributes that will assure continued growth of the R-SoXS and R-SoXR method and applications in a wide range of fields.

Most of the initial R-SoXS/R-SoXR developments utilized a bending magnet beamline at the Advanced Light Source (ALS) in Berkeley [57]. More recently, a much improved facility has been developed at an undulator beamline at the ALS [58,59].

This beamline offers higher flux and polarization control. The new facility also uses a 2D detector for more efficient solid angle coverage. Some work has also been performed with the BEAR instrument at Elettra [60] and beamline 4.0.1. at the ALS [61].

Work near the carbon edge is notoriously difficult, as most of the time the beamline optics is contaminated with carbon. This can lead to significant loss in incident intensity, the so-called "carbon dip", at energies that are most interesting from the application perspective. Concomitant with the loss of intensity for the fundamental energy of interest, the beam is enriched with higher spectral orders that can cause artifacts and systematic errors. Special attention has to be paid to a number of issues in order to get quantitative data. This includes the use of an order suppressor, periodic cleaning of the beamline optics, detector readout corrections, and tiling for extended q-range acquisition. The potential for radiation damage [58], which can causes significant mass loss or spectral changes [62] is also a concern. Further improvements in large solid angle detectors with increased dynamic range are highly desirable. For additional details and discussion of these topics in more depth, the reader is referred to the literature [59].

Unlike the situation in microscopy, where edges of samples are of little consequence and rather small samples can be studied with ease, edges introduce strong unwanted parasitic scattering if the sample is smaller than the photon beam. This parasitic scattering might limit the range of samples that can be investigated with R-SoXS until more tightly focused X-rays beams become available.

There are several soft X-ray scattering facilities existing or under construction at synchrotron facilities around the world, including efforts at SOLEIL, Electra, and the NSLS-II. However, not all of these facilities are specifically designed to characterize organic soft matter and so aren't necessarily concerned with carbon contamination and the numerous problems it creates. Our hope is that the advantages of using energies near the carbon edge to characterize organic materials will be more broadly recognized so that in time, more facilities can be readily used in the 250–320 eV energy range. The research opportunities seem to be plentiful.

5 Conclusions

By utilizing the selective contrast to composition and orientation afforded by the use of specific photon energies near the carbon absorption edge, R-SoXS and R-SoXR are proving very valuable in revealing structure-property relationships in organic matter and materials that range from solar cells, thin film transistors, light emitting diodes to block copolymer thin film samples, low k-dielectric materials and structured nano-particles. Most applications of R-SoXS/R-SoXR of organic matter to date have focused on characterizing synthetic materials. Similar to other scattering methods, R-SoXS is however a general characterization method that we expect to be used in many disciplines and across many materials classes. We anticipate a development similar to what has occurred in the field of transmission NEXAFS microscopy, which has initially been demonstrated utilizing polymers [22,63,64], and which has subsequently extended its reach to include for example, geological [65,66], magnetic [34,67], and biological materials. R-SoXS should in time also include applications on biological, environmental and organic geochemical materials.

This work was supported by the US Department of Energy, Office of Science, Basic Energy Science, Division of Materials Science and Engineering under contract DE-FG02-98ER45737. The author thanks C. R. McNeill (Monash U.) and T. Schuttford (Cambridge) for providing the CYTOP/P(NEI2OD-T2) sample and Hongping Yan (NCSU) for providing Fig. 4.

References

1. S. Günes, H. Neugebauer, N.S. Sariciftci, Chemical Reviews **107**, 1324 (2007)
2. A.V. Ruzette, L. Leibler, Nature Mater. **4**, 19 (2005)
3. R.J. Roe, *Methods of X-ray and Neutron Scattering in Polymer Science* (Oxford University Press, New York, 2000)
4. N. Stribeck, *X-ray scattering of soft matter* (Springer, 2007)
5. J.B. Kortright, D.D. Awschalom, J. Stöhr, S.D. Bader, Y.U. Idzerda, S.S.P. Parkin, I.K. Schuller, H.-C. Siegmann, J. Magn. Magn. Mater. **207**, 7 (1999)
6. C. Wang, T. Araki, H. Ade, Appl. Phys. Lett. **87**, 214109 (2005)
7. G.E. Mitchell, B.G. Landes, J. Lyons, B.J. Kern, M.J. Devon, I. Koprinarov, E.M. Gullikson, J.B. Kortright, Appl. Phys. Lett. **89**, 044101 (2006)
8. T. Araki, H. Ade, J.M. Stubbs, D.C. Sundberg, G. Mitchell, J.B. Kortright, A.L.D. Kilcoyne, Appl. Phys. Lett. **89**, 124106 (2006)
9. J.M. Virgili, Y.F. Tao, J.B. Kortright, N.P. Balsara, R.A. Segalman, Macromolecules **40**, 2092 (2007)
10. C. Wang, T. Araki, B. Watts, S. Harton, T. Koga, S. Basu, H. Ade, J. Vac. Sci. Technol. A **25**, 575 (2007)
11. S. Swaraj, C. Wang, T. Araki, G. Mitchell, L. Liu, S. Gaynor, B. Deshmukh, H. Yan, C.R. McNeill, H. Ade, Eur. Phys. J. Special Topics **167**, 121 (2009)
12. H. Ade, A.P. Hitchcock, Polymer **49**, 643 (2008)
13. C. Wang, A. Garcia, H. Yan, K.E. Sohn, A. Hexemer, T.-Q. Nguyen, G.C. Bazan, E.J. Kramer, H. Ade, J. Am. Chem. Soc. **131**, 12538 (2009)
14. S.P. Singh, M.H. Modi, P. Srivastava, Appl. Phys. Lett. **97**, 151906 (2010)
15. M. Nayak, G.S. Lodha, T.T. Prasad, P. Nageswararao, A.K. Sinha, J. Appl. Phys. **107**, 023529 (2010)
16. P. Gupta, A.K. Sinha, M.H. Modi, S.M. Gupta, P.K. Gupta, S.K. Deb, Appl. Surf. Sci. **257**, 210 (2010)
17. M. Nayak, G.S. Lodha, A.K. Sinha, R.V. Nandedkar, S.A. Shivashankar, Appl. Phys. Lett. **89**, 181920 (2006)
18. Y.S. Ding, S.R. Hubbard, K.O. Hodgson, R.A. Register, and S.L. Cooper, Macromolecules **21**, 1698 (1988)
19. B. Guilleaume, J. Blaul, M. Ballauff, M. Wittemann, M. Rehahn, G. Goerigk, Eur. Phys. J. E **8**, 299 (2002)
20. L.C. Davis, Phys. Rev. B **25**, 2912 (1982)
21. J. Daillant, Curr. Opinion Coll. Interf. Sci. **14**, 396 (2009)
22. H. Ade, X. Zhang, S. Cameron, C. Costello, J. Kirz, S. Williams, Science **258**, 972 (1992)
23. H. Ade, A.P. Smith, S. Cameron, R. Cieslinski, G. Mitchell, B. Hsiao, E. Rightor, Polymer **36**, 1843 (1995)
24. M. Mezger, B. Jérôme, J. Kortright, M. Valvidares, E. Gullikson, A. Giglia, N. Mahne, S. Nannarone, Phys. Rev. B **83**, 155406 (2011)
25. O. Dhez, H. Ade, S.G. Urquhart, J. Electron. Spectrosc. **128**, 85 (2003)
26. J. Kikuma, B.P. Tonner, J. Electron Spectros. Relat. Phenom. **82**, 53 (1996)
27. B. Watts, S. Swaraj, D. Nordlund, J. Luning, H. Ade, J. Chem. Phys. **134**, 024702 (2011)
28. S.G. Urquhart, H. Ade, J. Phys. Chem. B **106**, 8531 (2002)
29. P.L. Cook, X.S. Liu, W.L. Yang, F.J. Himpsel, J. Chem. Phys. **131** (2009)
30. S.G. Urquhart, A.P. Smith, H.W. Ade, A.P. Hitchcock, E.G. Rightor, W. Lidy, J. Phys. Chem. B **103**, 4603 (1999)
31. S.G. Urquhart, A.P. Hitchcock, A.P. Smith, H.W. Ade, E.G. Rightor, J. Phys. Chem. B **101**, 2267 (1997)
32. S. Swaraj, C. Wang, H. Yang, B. Watts, J. Lüning, C.R. McNeill, H. Ade, Nano Lett. **10**, 2863 (2010)
33. D. Chen, F. Liu, C. Wang, A. Nakahara, T.P. Russell, Nano Lett. **11**, 2071 (2011)
34. H. Ade, H. Stoll, Nature Materials **8**, 281 (2009)

35. W. Chen, T. Xu, F. He, W. Wang, C. Wang, J. Strzalka, Y. Liu, J. Wen, D.J. Miller, J. Chen, K. Hong, L. Yu, S.B. Darling, Nano Letters **11**, 3707 (2011)
36. H. Yan, S. Swaraj, C. Wang, I. Hwang, N.C. Greenham, C. Groves, H. Ade, C.R. McNeill, Adv. Funct. Mater. **20**, 4329 (2010)
37. H. Yan, C. Wang, A.R. McCarn, H. Ade, J. Opt. Soc. A (under review) (2012)
38. H. Yan, B.A. Collins, E. Gann, C. Wang, H. Ade, C.R. McNeill, ACS Nano **6**, 677 (2012)
39. H. Yan, T. Schuettfort, C.R. McNeill, H.W. Ade (in preparation) (2012)
40. O. Glatter, O. Kratky, *Small angle X-ray scattering* (Academic Press, New York, 1982)
41. J. Kido, M. Kimura, K. Nagai, Science **267**, 1332 (1995)
42. M.T. Bernius, M. Inbasekaran, J. O'Brien, and W. S. Wu, Adv. Mater. **12**, 1737 (2000)
43. W.L. Ma, P.K. Iyer, X. Gong, B. Liu, D. Moses, G.C. Bazan, A.J. Heeger, Adv. Mater. **17**, 274 (2005)
44. X. Gong, S. Wang, D. Moses, G.C. Bazan, A.J. Heeger, Adv. Mater. **17**, 2053 (2005)
45. R. Yang, H. Wu, Y. Cao, G.C. Bazan, J. Am. Chem. Soc. **128**, 14422 (2006)
46. H. Ade, C. Wang, A. Garcia, H. Yan, K.E. Sohn, A. Hexemer, G.C. Bazan, T.Q. Nguyen, E.J. Kramer, J. Polym. Sci. Part B: Polymer Physics **47**, 1291 (2009)
47. H. Yan, C. Wang, A. Garcia, S. Swaraj, Z. Gu, C.R. McNeill, T. Schuettfort, K.E. Sohn, E.J. Kramer, G.C. Bazan, T.-Q. Nguyen, H. Ade, J. Appl. Phys. **110**, 102220 (2011)
48. D.W. Steuerman, A. Garcia, M. Dante, R. Yang, J.P. Lofvander, T.Q. Nguyen, Adv. Mater. **20**, 528 (2008)
49. H. Yan, Z.H. Chen, Y. Zheng, C. Newman, J.R. Quinn, F. Dotz, M. Kastler, A. Facchetti, Nature **457**, 679 (2009)
50. J. Rivnay, M.F. Toney, Y. Zheng, I.V. Kauvar, Z. Chen, V. Wagner, A. Facchetti, A. Salleo, Adv. Mater. **22**, 4359 (2010)
51. J. Stöhr, *Nexafs spectroscopy* (Springer-Verlag, New York, 1992)
52. B.A. Collins, J. Cochran, H. Yan, E. Gann, C. Hub, R. Fink, C. Wang, T. Schuettfort, C.R. McNeill, M.L. Chabinyc, H. Ade, Nature Materials, DOI: 10.1038/NMAT3310 (2012)
53. B.A. Collins, J. Tumbleston, H. Ade, J. Phys. Chem. Lett. **2**, 3135 (2011)
54. Z. He, C. Zhong, X. Huang, W.-Y. Wong, H. Wu, L. Chen, S. Su, Y. Cao, Adv. Mater. **23**, 4636 (2011)
55. E. Pavlopoulou, S.H. Anastasiadis, J.B. Kortright, W. Bras, G. Portale, IOP Conf. Ser.: Mater. Sci. Eng. **14**, 012017 (2010)
56. C. Wang, D.H. Lee, A. Hexemer, M.I. Kim, W. Zhao, H. Hasegawa, H. Ade, T.P. Russell, Nano Lett. **11**, 3906 (2011)
57. J.H. Underwood, E.M. Gullikson, J. Electron. Spectrosc. **92**, 265 (1998)
58. C. Wang, A. Hexemer, J. Nasiatka, E.R. Chan, A.T. Young, H.A. Padmore, W.F. Schlotter, J. Lüning, S. Swaraj, B. Watts, E. Gann, H. Yan, H. Ade, IOP Conf. Ser.: Mater. Sci. Eng. **14**, 012016 (2010)
59. E. Gann, A. Young, B.A. Collins, H. Yan, J. Nasiatka, H.A. Padmore, H. Ade, A. Hexemer, C. Wang, Rev. Sci. Instrum. **83**, 045110 (2012)
60. S. Nannarone, F. Borgatti, A. DeLuisa, B.P. Doyle, G.C. Gazzadi, A. Giglia, P. Finetti, N. Mahne, L. Pasquali, M. Pedio, G. Selvaggi, G. Naletto, M.G. Pelizzo, G. Tondello, in *Synchrotron radiation instrumentation*, edited by T. Warwick, J. Arthur, H.A. Padmore et al. (2004), vol. 705, p. 450
61. A.T. Young, J. Feng, E. Arenholz, H.A. Padmore, T. Henderson, S. Marks, E. Hoyer, R. Schlueter, J.B. Kortright, V. Martynov, C. Steier, G. Portmann, Nucl. Instrum. Meth. A **467**, 549 (2001)
62. T. Coffey, S.G. Urquhart, H. Ade, J. Electron Spectrosc. Relat. Phenom **122**, 65 (2002)
63. H. Ade, B. Hsiao, Science **262**, 1427 (1993)
64. S. Zhu, Y. Liu, M.H. Rafailovich, J. Sokolov, D. Gersappe, D.A. Winesett, H. Ade, Nature **400**, 49 (1999)
65. D. Papineau, B.T. De Gregorio, G.D. Cody, J. O/'Neil, A. Steele, R.M. Stroud, M.L. Fogel, Nature Geosci. **4**, 376 (2011)

66. C.D.K. Herd, A. Blinova, D.N. Simkus, Y. Huang, R. Tarozo, C.M.O. D. Alexander, F. Gyngard, L.R. Nittler, G.D. Cody, M.L. Fogel, Y. Kebukawa, A.L.D. Kilcoyne, R.W. Hilts, G.F. Slater, D.P. Glavin, J.P. Dworkin, M.P. Callahan, J.E. Elsila, B.T. De Gregorio, R.M. Stroud, Science **332**, 1304 (2011)
67. B. Van Waeyenberge, A. Puzic, H. Stoll, K.W. Chou, T. Tyliszczak, R. Hertel, M. Fähnle, H. Brückl, K. Rott, G. Reiss, I. Neudecker, D. Weiss, C.H. Back, G. Schütz, Nature **444**, 461 (2006)
68. C.K. Boyce, M.A. Zwieniecki, G.D. Cody, C. Jacobsen, S. Wirick, A.H. Knoll, N.M. Holbrook, P. Natl. Acad. Sci. USA. **101**, 17555 (2004)